Mean-field interactions between living cells in linear and nonlinear elastic matrices

Chaviva Sirote[1] and Yair Shokef[2,3,4,*]

[1]*Department of Biomedical Engineering, Tel Aviv University, Tel Aviv 69978, Israel*
[2]*School of Mechanical Engineering, Tel Aviv University, Tel Aviv 69978, Israel*
[3]*Sackler Center for Computational Molecular and Materials Science, Tel Aviv University, Tel Aviv 69978, Israel*
[4]*Center for Physics and Chemistry of Living Systems, Tel Aviv University, Tel Aviv 69978, Israel*

(Received 26 April 2021; revised 15 July 2021; accepted 28 July 2021; published 12 August 2021)

Living cells respond to mechanical changes in the matrix surrounding them by applying contractile forces that are in turn transmitted to distant cells. We consider simple effective geometries for the spatial arrangement of cells, we calculate the mechanical work that each cell performs in order to deform the matrix, and study how that energy changes when a contracting cell is surrounded by other cells with similar properties and behavior. Cells regulating the displacements that they generate are attracted to each other in a manner that does not depend on the cell's rigidity. Whereas cells regulating the active stress that they apply repel each other. This repulsion depends on the cell's bulk modulus in spherical geometry, while in cylindrical geometries the interaction depends also on their shear modulus. In nonlinear, strain-stiffening matrices, for displacement regulation, in the presence of other cells, cell contraction is limited due to the divergence of the shear stress. For stress regulation, the interaction energy drops at the nonlinear stiffening stress. Our theoretical work provides insight into matrix-mediated interactions between contractile cells and on the role of their mechanical regulatory behavior.

DOI: 10.1103/PhysRevE.104.024411

I. INTRODUCTION

Living cells embedded in, or adhered on an elastic environment transmit mechanical forces through deformations of their surrounding solid medium [1]. Thus their active contraction may be felt by non-contacting cells through the propagation of stress and strain fields via this matrix. Such mechanical interactions between cells and their surrounding environments, as well as matrix-mediated cell-cell interactions are important for many biological processes, such as stem-cell differentiation [2], wound healing [3], embryonic development [4], cell division [5,6], cancer metastasis [7,8], and cell-cell biochemical communication [9–11]. Recent experiments in synthetic setups or geometries enable to isolate and study these mechanical interactions [12–17].

Theoretically, cell contraction is customarily modeled by assuming that cells generate active force dipoles [18], namely, that they apply on the elastic medium pairs of equal-magnitude and oppositely pointing forces. The interaction between distant such force dipoles may be described in terms of the excess elastic energy stored in the medium in a situation with interacting cells compared to the total energy of these cells without interactions. Interaction energies between active force dipoles have been studied in the past in the context of atoms adsorbed to surfaces [19], and more recently in the cell mechanics context, with studies ranging from simple, linear dipoles comprising pairs of point forces [20–25] to more complex continuous shapes [26].

To simplify the description of actively contractile cells, cells within a three-dimensional medium [5,17] have been modeled as spherical force dipoles [27–30]. Namely, the mechanical activity of each cell is described by an isotropic distribution of radial external forces that are applied on the surface of a sphere within a three-dimensional elastic medium. This may be thought of as a continuous collection of linear force dipoles distributed isotropically on the surface of this sphere, with each such linear force dipole applying equal and opposite forces at two opposing points on the sphere. This spherical geometry implies spherical symmetry for the elastic fields around a cell and thus simplifies the partial differential equations of elastic equilibrium that should be solved to a one-dimensional or ordinary differential equation for the radial displacement as a function of the radial coordinate. We note that this model should be thought of as a representation of an effective geometry. If the cell would simply contract isotropically as in our simplified model, its volume would change, which is not consistent with the fact that actual cells are nearly incompressible. Instead, our geometry should be thought of as an effective description for the more complex realistic situation in which cell contraction is very anisotropic. Having said that, there are experiments of relatively symmetric fibroblast cells exhibiting contraction in three-dimensional fibrin gels in the first hours after seeding the cells in the gel [17,31] or of cancer cells contracting isotropically in collagen gels [32].

Along the lines of the aforementioned theoretical modeling, interactions between biological cells have been modeled by imposing a zero-displacement boundary condition at some distance from this spherical cell [29]. The justification for this is to first assume that the spatial distribution of cells in their elastic environment is on a periodic array. In such case, by symmetry, the normal displacement on the surface of each periodic unit cell of this array should vanish. A reasonable

*shokef@tau.ac.il; https://shokef.tau.ac.il

mean-field approximation would then be to replace the actual polyhedral periodic unit cell with a spherical unit cell with zero displacement on its boundary, which results in a simple one-dimensional geometry also for the study of cell-cell interactions. Note that the periodic unit cell of an array of biological cells and the spherical domain approximating this unit cell should not be confused with the biological cells.

Cell-cell elastic interactions are similar, but not identical to electrostatic interactions between induced electric dipoles [1,18,23,33,34], and the interaction energy scales algebraically with distance. Interestingly, the sign of the interaction energy is set by the homeostatic behavior of the cells; cells regulating the displacement on their boundary repel each other, and cells regulating the force that they apply are mechanically attracted to each other [29]. Elaborate solutions, which include the interference between the angular dependence of the deformation fields around two spheres recover these mean-field results, in terms both of the sign and of the exponents of the power-law decay in the magnitude of the interaction energy [34].

In this paper we use the mean-field approach described above to study additional geometries, namely, not only spherical symmetry, but also two simple cylindrical setups [35] that relate to cells on substrates or to elongated cells in a three-dimensional matrix. In doing that, we provide further insight on matrix-mediated elastic interactions in more complex geometries, for which analytical results are not known. Furthermore, we include in our calculations the stiffness of the interior the cell, and not only that of the surrounding matrix. Finally, and most importantly, we extend our analysis to cells in nonlinear, strain-stiffening media [27].

II. MODEL AND INTERACTION ENERGY

We analyze two geometries, one in which the contracting cell is assumed to be a sphere of radius R_0, and the other in which it is assumed to be a cylinder of radius R_0. In both geometries, we model the presence of neighboring cells by imposing a rigid wall with zero normal displacement at some larger radius R_1; see Fig. 1. This radius represents half of the distance to nearby cells, since in realistic geometries, by symmetry the normal displacement should vanish at that position. In our model, the biological cell has linear elastic response characterized by shear modulus μ_c and bulk modulus K_c. In Sec. III we will assume that the matrix is also linearly elastic with shear modulus μ_m and bulk modulus K_m, while in Sec. IV we will include nonlinear strain stiffening of the matrix.

The elastic energy stored in the cell and in the matrix together is equal to the mechanical work performed by the active, or external forces, which act only at the surface of the cell. Here these are radial forces that act at the radius R_0 and generate a radial displacement u_0 there. We assume that in the absence of these active forces, the elastic medium is relaxed, and hence we calculate the work done on the matrix by integrating over the adiabatic process of building up the displacement u_0, starting from this relaxed state [26]

$$E = \int_0^{u_0} g\tau(w)\,dw. \tag{1}$$

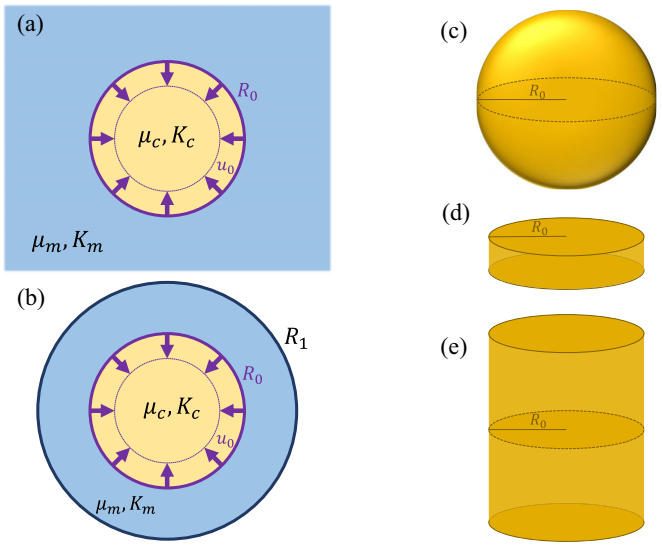

FIG. 1. Schematic of a single cell in an infinite matrix (a) and in a bounded region (b). The cell may be a sphere (c), a flat cylinder (d) for plane stress, or a long cylinder (e) for plane strain.

Here w denotes the displacement at R_0 during this process, and $\tau(w) = \sigma_c(R_0) - \sigma_m(R_0)$ is the active stress applied by the cell, namely the discontinuity in the radial component of the stress tensor on the surface of the cell when the displacement there is equal to w. We use σ_c and σ_m to denote the radial component σ_{rr} of the stress tensor in the cell and in the matrix, respectively. The geometrical factor relating stress to force is equal to $g = 4\pi R_0^2$ in the spherical geometry. In the cylindrical geometry we use $g = 2\pi R_0$ to obtain the force per unit length of the cylinder and subsequently the energy per unit length. Since much of our analysis and discussion below is performed simultaneously for the two geometries, for brevity we will use the term energy and the symbol E for energy in the spherical geometry and for energy per unit length in the cylindrical geometry. If the medium is linearly elastic (Sec. III), there is a linear proportionality between displacement and active stress, $\tau(w) \propto w$, and Eq. (1) reduces to $E = \frac{1}{2} g\sigma_0 u_0$, where $\sigma_0 = \tau(u_0)$ is the active stress, or stress difference on the surface of the cell when the displacement there is equal to u_0 [29,34]. However, for nonlinear media (Sec. IV), the entire dependence of τ on w up to the actual displacement u_0 is required in order to perform the integration in Eq. (1).

We define the interaction energy as the added work that the cell has to perform due to the presence of neighboring cells. Within our mean-field approximation, this is equal to the difference

$$\Delta E = E_1 - E_\infty \tag{2}$$

between the elastic energy E_1 stored in the medium when there is a zero-displacement boundary condition at R_1 [Fig. 1(b)] and the elastic energy E_∞ of the same cell in an unbounded matrix [Fig. 1(a)]. Care should be given to the meaning of this placement of the same cell in two different mechanical environments. Obviously when identical cells have different environments, they behave differently [2,36–41]. In our case, the confining geometry alters the re-

lation between the active stress τ and the displacement u_0. Thus cells in the confined and in the unbounded geometries cannot simultaneously have both the same active stress and the same deformation. We will consider two extreme scenarios: (1) displacement regulation, for which cells are assumed to be biologically programed to generate a given displacement u_0, regardless of what active stress they need to apply in order to reach that deformation and (2) stress regulation, for which cells apply a given active stress σ_0, regardless of the displacement they manage to generate.

For cells regulating the displacement on their surface, the far-field zero-displacement boundary condition imposed by the presence of neighboring cells causes cells to apply a larger active stress in order to generate a given contraction. Thus we expect the interaction energy to be positive, representing repulsion between cells. For stress regulation, on the other hand, a smaller displacement will be generated in the presence of other cells, thus leading to a negative interaction energy, or to attraction [29,34]. We consider cells that are embedded in a solid surrounding; thus they cannot easily move due to these repulsive or attractive interactions. However, we suggest that these interactions are the mechanical cause for instance for cells to send protrusions one toward each other or rather away from each other [15] or for cells to generate bands of densification and alignment of the network of fibers around them [9,31], and also for migratory behavior of cells on substrates [12]. Alternatively, our results could be used to explain when do cells regulate their displacement and when do they regulate their active stress, depending on the energetic cost for doing so.

Our strategy for calculating the interaction energy for the different cases described above is as follows: We first assume a displacement u_0 on the boundary of the cell, and solve for the displacement field. Using the resulting strain, we calculate the stress on the boundary of the cell, and from that the active stress σ_0 that the cell has to apply to generate the displacement u_0. We then use these to calculate the elastic energy stored in the deformation. For displacement regulation we subtract the resulting energies in the bounded and in the unbounded geometries to get the interaction energy, Eq. (2) at a given displacement u_0. For stress regulation, we combine our results for E versus u_0 and for σ_0 versus u_0 to obtain E versus σ_0, and then use Eq. (2) to get the interaction energy at a given active stress σ_0. This procedure has been applied previously [29] for an empty spherical cell in a linearly elastic medium, with the focus on the asymptotic behavior when cells are far apart from each other, which translates to $R_1 \gg R_0$ in our model. Here we provide the full dependence on distance, and also (1) include a passive, elastic rigidity of the interior of the cell, (2) solve for additional cases with cylindrical symmetry, and (3) study the effects of nonlinear elastic response of the matrix.

III. LINEAR MEDIUM

Our spherical and cylindrical geometries both assume radial symmetry, such that the displacement vector $\vec{u}(\vec{r}) = u(r)\hat{r}$ is given only by the radial component $u(r)$, which depends only on the radial coordinate r. In this section we assume that the mechanical response of both the cell and the surrounding matrix is linearly elastic. This leads to linear ordinary differential equations for $u(r)$, which we analytically solve. Thus we obtain exact analytical expressions for the interaction energy in the different geometries. More complicated nonlinear material models may be considered for the cell and for the matrix, for instance the nonlinear elastic response of the matrix as described in Sec. IV below. Such models result in nonlinear differential equations that need to be solved in order to obtain the displacement field. However, the spherical and cylindrical symmetries of our geometrical setups reduces the general three-dimensional partial differential equations of nonlinear elasticity to one-dimensional ordinary differential equations, which, if needed, may be solved numerically much more easily.

A. Spherical cell

For spherical symmetry [Fig. 1(c)], mechanical equilibrium implies [42]

$$\frac{d^2u}{dr^2} + \frac{2}{r}\frac{du}{dr} - \frac{2u}{r^2} = 0. \tag{3}$$

The general solution to this equation is

$$u(r) = Cr + \frac{D}{r^2}, \tag{4}$$

where the constants C and D are set by the boundary conditions. For spherical symmetry, the radial stress is given by [42]

$$\sigma_{rr} = \frac{4}{3}\mu\left(\frac{du}{dr} - \frac{u}{r}\right) + K\left(\frac{du}{dr} + \frac{2u}{r}\right), \tag{5}$$

which for the general solution (4) may be written as

$$\sigma_{rr} = 3KC - \frac{4\mu D}{r^3}. \tag{6}$$

Thus for spherical symmetry, the $u \propto r$ term in (4) represents pure compression, while the $u \propto 1/r^2$ term represents pure shear.

Inside the cell ($0 < r < R_0$) the boundary conditions are $u(0) = 0$ and $u(R_0) = u_0$; thus the displacement is given by

$$u_c = \frac{u_0 r}{R_0}, \tag{7}$$

which contains only compression, and the stress in the cell is uniform and equal to

$$\sigma_c = 3K_c\frac{u_0}{R_0}, \tag{8}$$

which depends only on the bulk modulus of the cell and not on its shear modulus.

In the surrounding matrix ($r > R_0$), the displacement at the cell border is $u(R_0) = u_0$. For the unbounded case, the second boundary condition is that $u = 0$ at $r = \infty$, leading to

$$u_{m,\infty} = \frac{u_0 R_0^2}{r^2}, \tag{9}$$

which contains only shear. The stress in the matrix in this case is thus

$$\sigma_{m,\infty} = -\frac{4\mu_m u_0 R_0^2}{r^3} = -4\mu_m\frac{u_0}{R_0}, \tag{10}$$

where the second equality is obtained by setting the position to be on the surface of the cell, $r = R_0$. The total work that an isolated cell performs in order to deform both itself and the matrix that surrounds it is thus

$$E_\infty = 2\pi u_0^2 R_0 (3K_c + 4\mu_m). \tag{11}$$

For the bounded case, the second boundary condition is now $u(R_1) = 0$, and the displacement in the matrix is

$$u_{m,1} = \frac{u_0 R_0^2}{R_1^3 - R_0^3}\left(\frac{R_1^3}{r^2} - r\right), \tag{12}$$

which contains both shear and compression. In this case, the stress in the matrix is

$$\sigma_{m,1} = -\frac{4\mu_m R_1^3 + 3K_m R_0^3}{R_1^3 - R_0^3}\frac{u_0}{R_0}, \tag{13}$$

and the energy is

$$E_1 = 2\pi u_0^2 R_0 \left[3K_c + \frac{4\mu_m R_1^3 + 3K_m R_0^3}{R_1^3 - R_0^3}\right]. \tag{14}$$

1. Displacement regulation

If the cell generates the same displacement u_0 on its boundary regardless of its mechanical environment, the interaction energy is just the difference between the energy (14) when it is bounded and the energy (11) when it is unbounded, namely,

$$\Delta E = E_1 - E_\infty = 2\pi u_0^2 R_0^4 \frac{4\mu_m + 3K_m}{R_1^3 - R_0^3}. \tag{15}$$

This result depends on both the bulk and shear moduli of the matrix because both compression and shear are generated in the matrix. It does not, however, depend on the elastic moduli of the cell since for displacement regulation, the cell deforms in the exact same way in the bounded and in the unbounded geometries; thus the same energy is stored in the cell for both geometries. As predicted above, for displacement regulation, the interaction energy is positive, representing repulsion between cell. For large separation between cell ($R_1 \gg R_0$), the interaction energy decays as $1/R_1^3$, which is consistent with a mapping to interactions between induced electric dipoles [29,34].

2. Stress regulation

If the cell generates the same active stress σ_0 both when it is bounded and when it is unbounded, we need to first express the energies E_1 and E_∞ in terms of σ_0 rather than u_0, and only then subtract them to get the interaction energy. Using Eqs. (10) and (8), for an unbounded cell, the displacement on its boundary is given by

$$u_{0,\infty} = \frac{\sigma_0 R_0}{3K_c + 4\mu_m}, \tag{16}$$

and from Eq. (11), the energy in this case is given by

$$E_\infty = \frac{2\pi\sigma_0^2 R_0^3}{3K_c + 4\mu_m}. \tag{17}$$

Similarly, from Eqs. (13) and (8), the displacement on the boundary of a bounded cell is

$$u_{0,1} = \frac{\sigma_0 R_0 \left(R_1^3 - R_0^3\right)}{4\mu_m R_1^3 + 3K_m R_0^3 + 3K_c\left(R_1^3 - R_0^3\right)}, \tag{18}$$

and the energy (14) in this case is

$$E_1 = \frac{2\pi\sigma_0^2 R_0^3 \left(R_1^3 - R_0^3\right)}{4\mu_m R_1^3 + 3K_m R_0^3 + 3K_c\left(R_1^3 - R_0^3\right)}. \tag{19}$$

By subtracting (17) from (19) we get that for stress regulation the interaction energy is

$$\Delta E = -\frac{2\pi\sigma_0^2 R_0^6 (4\mu_m + 3K_m)}{(4\mu_m + 3K_c)\left[4\mu_m R_1^3 + 3K_m R_0^3 + 3K_c\left(R_1^3 - R_0^3\right)\right]}. \tag{20}$$

As discussed above, for stress regulation, the interaction energy is negative, representing attraction between cells. Moreover, here the contraction of the cell differs between the bounded and unbounded geometries, therefore the interaction energy depends on the stiffness of the cell. However, for spherical symmetry the deformation of the cell includes only compression; thus the interaction energy depends on the bulk modulus of the cell but not on its shear modulus. The $1/R_1^3$ decay in the magnitude of the interaction energy for large distances between cells is similar to that found above for displacement regulation.

B. Cylindrical cell

For cylindrical symmetry, the boundary conditions at the ends of the cylinder affect the stress inside it. If the cylinder is prevented from deforming in the axial direction, the axial strain vanishes $\epsilon_{zz} = 0$, this is termed plane strain, and the radial stress reads [42]

$$\sigma_{rr}^A = \frac{2}{3}\mu\left(2\frac{du}{dr} - \frac{u}{r}\right) + K\left(\frac{du}{dr} + \frac{u}{r}\right). \tag{21}$$

In order to maintain this state, external axial forces should be applied at the ends of the cylinder. Note that there is no displacement there, hence these forces do not perform any work, and thus do not contribute to the energy. If such forces are not applied, the axial stress is zero $\sigma_{zz} = 0$, this is termed plane stress, and the radial stress is given by [42]

$$\sigma_{rr}^E = \frac{2}{3}\mu\left(2\frac{du}{dr} - \frac{u}{r}\right) + \frac{1 - 4\nu^2}{1 - \nu^2}K\left(\frac{du}{dr} + \frac{u}{r}\right), \tag{22}$$

with the Poisson ratio given by

$$\nu = \frac{3K - 2\mu}{2(3K + \mu)}. \tag{23}$$

Also for plane stress no work is done due to the axial deformation since no forces are applied in that direction. The simple geometries considered here are not meant to exactly describe the shapes of specific biological cells and their environments. However, we suggest that plane stress [Fig. 1(d)] may be more relevant for thin cells in a monolayer or for cells on a substrate, while plane strain [Fig. 1(e)] may be more relevant for elongated cells such as neurons, in a three-dimensional environment.

Regardless of the aforementioned boundary conditions in the axial direction, cylindrical symmetry implies that the radial displacement satisfies the following differential equation, which ensures mechanical equilibrium [42]

$$\frac{d^2u}{dr^2}+\frac{1}{r}\frac{du}{dr}-\frac{u}{r^2}=0. \tag{24}$$

The general solution to this equation reads

$$u(r)=Cr+\frac{D}{r}, \tag{25}$$

where the constants C and D are set by the boundary conditions in the radial direction. We now generalize the two cases for the axial boundary conditions, plane strain (21) and plane stress (22), to write the radial stress for both cases as

$$\sigma_{rr}=\frac{2}{3}\mu\left(2\frac{du}{dr}-\frac{u}{r}\right)+\hat{K}\left(\frac{du}{dr}+\frac{u}{r}\right), \tag{26}$$

with an effective bulk modulus given by

$$\hat{K}=\begin{cases}K & \text{plane strain}\\ \frac{1-4\nu^2}{1-\nu^2}K & \text{plane stress}\end{cases}. \tag{27}$$

Substituting the general solution for the displacement (25) in (26) enables us to generally write the stress as

$$\sigma_{rr}=2\mu\left(\frac{C}{3}-\frac{D}{r^2}\right)+2\hat{K}C. \tag{28}$$

From this we see that the solution $u=D/r$ contains only shear. However, as opposed to the spherical case discussed above, in cylindrical geometry, the solution $u=Cr$ contains both shear and compression.

Similarly to the procedure employed above for a spherical cell, we will now solve for the displacement field $u(r)$, from which we will obtain the relation between the displacement u_0 on the cell boundary and the active stress σ_0 that the cell applies, and from which we will calculate the elastic energy for a bounded and for an unbounded cell, and subsequently the interaction energy for displacement regulation and for stress regulation.

Inside the cell, the displacement has the same form as for the spherical geometry,

$$u_c=\frac{u_0 r}{R_0}. \tag{29}$$

Here, by Eq. (28), the stress inside the cell is given by

$$\sigma_c=\left(\frac{2}{3}\mu_c+2\hat{K}_c\right)\frac{u_0}{R_0}. \tag{30}$$

Outside the cell, for the unbounded cylindrical geometry, the displacement is

$$u_{m,\infty}=\frac{u_0R_0}{r}, \tag{31}$$

which leads to the following radial stress on the surface of the cell ($r=R_0$):

$$\sigma_{m,\infty}=-2\mu_m\frac{u_0}{R_0}, \tag{32}$$

and subsequently to the energy per unit length

$$E_\infty=2\pi u_0^2\left(\frac{\mu_c}{3}+\hat{K}_c+\mu_m\right). \tag{33}$$

It is interesting to note that E_∞ does not depend on the cell radius, R_0. For the bounded geometry, the displacement is given by

$$u_{m,1}=\frac{u_0R_0}{R_1^2-R_0^2}\left(\frac{R_1^2}{r}-r\right), \tag{34}$$

thus the stress on the surface of the cell reads

$$\sigma_{m,1}=-\frac{2u_0R_0}{R_1^2-R_0^2}\left[\mu_m\left(\frac{1}{3}+\frac{R_1^2}{R_0^2}\right)+\hat{K}_m\right], \tag{35}$$

and the energy per unit length is

$$E_1=\pi u_0^2\left\{\frac{2}{3}\mu_c+2\hat{K}_c+\left[\frac{2}{3}\mu_m\left(1+3\frac{R_1^2}{R_0^2}\right)+2\hat{K}_m\right]\frac{R_0^2}{R_1^2-R_0^2}\right\}. \tag{36}$$

As for the spherical case, for fixed displacement, we obtain the interaction energy by subtracting (33) from (36), leading to

$$\Delta E=\frac{2}{3}\pi u_0^2R_0^2\frac{4\mu_m+3\hat{K}_m}{R_1^2-R_0^2}. \tag{37}$$

Similarly to the procedure described above for spherical symmetry, also in cylindrical symmetry for regulation of the active stress, we use (30), (32), and (35) to obtain u_0 in terms of σ_0 for the bounded and for the unbounded cases, and from that obtain the interaction energy,

$$\Delta E=-\frac{\pi}{6}\sigma_0^2R_0^4\frac{4\mu_m+3\hat{K}_m}{\left(\mu_m+\frac{\mu_c}{3}+\hat{K}_c\right)\left[\left(\frac{\mu_m}{3}+\hat{K}_m\right)R_0^2+\mu_mR_1^2+\left(\hat{K}_c+\frac{\mu_c}{3}\right)\left(R_1^2-R_0^2\right)\right]}. \tag{38}$$

As for the spherical geometry, also for the cylindrical geometry we get for displacement regulation a repulsive interaction (37) which depends only on the elastic moduli of the matrix, while for stress regulation we obtain attractive interaction (38), which depends also on the elastic moduli of the cell. Here there is both shear and compression in the cell; thus (38) depends on both μ_c and K_c. For large separations between cells, $R_1\gg R_0$, the interaction energy in the cylindrical geometry decays as $1/R_1^2$, as opposed to $1/R_1^3$ in spherical geometry, which is consistent with the dimensionality reduction between the two cases.

IV. NONLINEAR MEDIUM

A. Nonlinear material model

The analysis presented in Sec. III assumes linear elasticity and is hence valid only for extremely small deformations. The extracellular matrix is a gel of crosslinked polymers, which

exhibits nonlinear mechanical response; its response to shear is linear at small stress, while for higher stress, the differential shear modulus crosses over to a power-law increase with shear stress, $G(\sigma) \propto \sigma^{3/2}$ [43–46]. The nonlinearity of the material may be quantified by the strain where this crossover occurs. Due to their near-incompressibility, biopolymer gels are usually compressed much less than they are sheared; thus we shall include nonlinearity only in their response to shear. Specifically, we describe the nonlinear medium surrounding our cells using the following energy density function [27]:

$$W = \frac{\mu}{2}\left\{[1 - b(\bar{I}_1 - 3)]^{-1} - 1\right\} + \frac{K}{2}(J-1)^2, \tag{39}$$

where μ and K are the shear and bulk moduli in the linear regime, and b is a dimensionless parameter quantifying the strength of the nonlinearity. The second term describes compression in a neo-Hookean manner with $J = \det(\mathbf{F})$ quantifying the compression, and $F_{i,j} = \partial x_i/\partial X_j$ the deformation gradient tensor, where $\vec{X}$ is the reference position and $\vec{x}$ the deformed position. The first term in (39) describes shear with $\bar{I}_1 = \mathrm{tr}(\mathbf{B})/J^{2/3}$ the normalized first eigenvalue of the left Cauchy-Green strain tensor, $\mathbf{B} = \mathbf{F}\mathbf{F}^T$. Most generally, the Cauchy stress tensor is derived from the energy density as

$$\sigma_{ij} = \frac{1}{J} F_{ik} \frac{\partial W}{\partial F_{kj}}. \tag{40}$$

However, for an energy density function which depends only on J and I_1, this reduces to [42]

$$\boldsymbol{\sigma} = \frac{2}{J^{5/3}} \frac{\partial W}{\partial \bar{I}_1}\left(\mathbf{B} - \frac{I_1}{3}\mathbf{1}\right) + \frac{\partial W}{\partial J}\mathbf{1}, \tag{41}$$

with $\mathbf{1}$ the unit tensor. For our model (39), this yields

$$\boldsymbol{\sigma} = \frac{\mu}{J^{5/3}}[1 - b(\bar{I}_1 - 3)]^{-2}\left(\mathbf{B} - \frac{I_1}{3}\mathbf{1}\right) + K(J-1)\mathbf{1}. \tag{42}$$

For simple shear, the deformation may be written as $x = X + \gamma Z$, $y = Y$, $z = Z$; thus Eq. (42) gives a shear stress of $\sigma_{xz} = \mu\gamma(1 - b\gamma^2)^{-2}$, resulting in the differential shear modulus $G \equiv d\sigma/d\gamma = \mu(1 + 3b\gamma^2)(1 - b\gamma^2)^{-3}$. In the limit of small shear ($\gamma \ll 1$), we obtain linear response $\sigma \approx \mu\gamma$ with a constant differential shear modulus equal to μ. For large shear, the shear stress σ_{xz} diverges as the strain γ approaches a maximal possible strain $\gamma_a = 1/\sqrt{b}$. In that limit of $\sigma \gg \mu\gamma_a$, the differential shear modulus may be approximated as $G \approx 4\mu[\sigma/(\mu\gamma_a)]^{3/2}$, which exhibits the power-law stiffening $G \propto \sigma^{3/2}$ characteristic of biopolymer gels; see Fig. 2.

Below we will study the effects of this power-law stiffening on matrix mediated elastic interactions between cells. We will consider the same geometrical model studied above, of a symmetric contracting cell, surrounded by an effective wall, which provides a mean-field description for the effect of neighboring cells. For simplicity, we will restrict ourselves to a spherical cell. However, the extensions described above for for cylindrical cells are straightforward.

In order to simplify the analysis, we will restrict ourselves to the small deformations limit, which is relevant for strongly nonlinear materials ($b \gg 1$) that have a very small maximal shear strain $\gamma_a \ll 1$. As shown in [27], the nonlinearity of biological gels has $2 < b < 400$, or an equivalently maximal

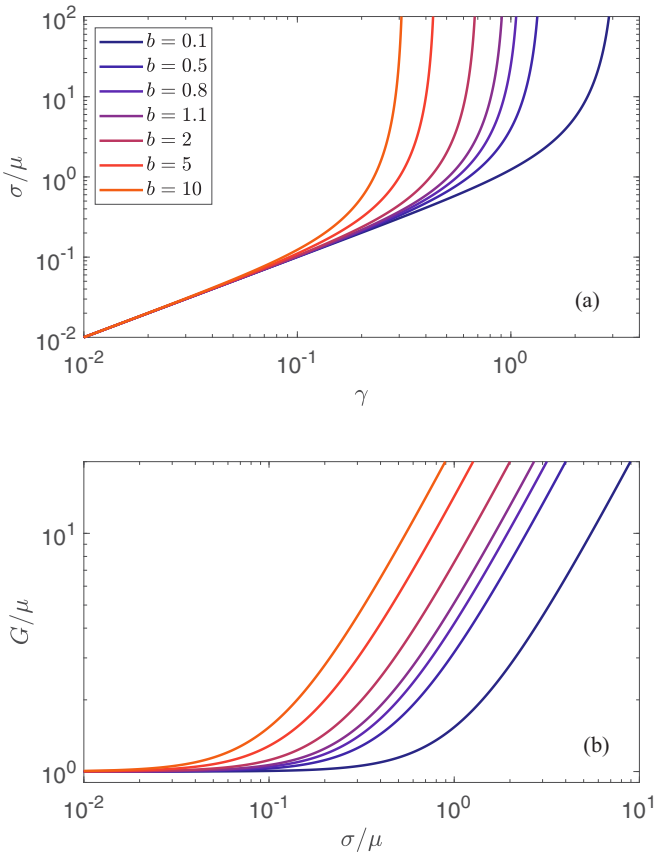

FIG. 2. Stress stiffenning for simple shear: (a) Stress vs strain is linear for small strain and then diverges at $\gamma_a = 1/\sqrt{b}$. (b) Differential shear modulus is constant for small stress and then increases as $G \propto \sigma^{3/2}$ for stress larger than $\mu\gamma_a$.

shear strain of $0.05 < \gamma_a < 0.7$. In such cases, the deformations will always be small $\gamma \ll 1$, and we will have strong nonlinear effects even at small deformations. In our spherical case, this implies $u/r, du/dr \ll 1$. We will obviously keep terms linear in u. However, since for simple shear $b = 1/\gamma_a^2$, for consistency, we will keep also terms proportional to bu^2, and will neglect only terms that are higher order than that.

For spherical symmetry, the deformation is described by the difference $u(R) = r(R) - R$ between the deformed radius r and the reference radius R. The compression and shear components of the deformation are generally given by [42]

$$\begin{aligned} J &= \left(1 + \frac{u}{R}\right)^2\left(1 + \frac{du}{dR}\right), \\ \bar{I}_1 &= \left(1 + \frac{u}{R}\right)^{-4/3}\left(1 + \frac{du}{dR}\right)^{4/3} \\ &\quad + 2\left(1 + \frac{u}{R}\right)^{2/3}\left(1 + \frac{du}{dR}\right)^{-2/3}. \end{aligned} \tag{43}$$

For small displacements ($u \ll R$), these are approximated as

$$\begin{aligned} J &\approx 1 + 2\frac{u}{r} + \frac{du}{dr}, \\ \bar{I}_1 - 3 &\approx \frac{4}{3}\left(\frac{du}{dr} - \frac{u}{r}\right)^2, \end{aligned} \tag{44}$$

where we have also used the small deformation approximation to replace R with r.

Force balance $\nabla \cdot \boldsymbol{\sigma} = 0$ implies

$$\frac{d\sigma_{rr}}{dr} + \frac{2}{r}(\sigma_{rr} - \sigma_{\theta\theta}) = 0. \tag{45}$$

In spherical coordinates, the general expression for the stress tensor (41) gives

$$\sigma_{rr} = \frac{4}{3J^{5/3}}\frac{\partial W}{\partial \bar{I}_1}\left[\left(\frac{du}{dr}\right)^2 + 2\frac{du}{dr} - \left(\frac{u}{r}\right)^2 - 2\frac{u}{r}\right] + \frac{\partial W}{\partial J},$$
$$\sigma_{rr} - \sigma_{\theta\theta} = \frac{2}{J^{5/3}}\frac{\partial W}{\partial \bar{I}_1}\left[\left(\frac{du}{dr}\right)^2 + 2\frac{du}{dr} - \left(\frac{u}{R}\right)^2 - 2\frac{u}{r}\right], \tag{46}$$

where for our strain energy density (39),

$$\frac{\partial W}{\partial \bar{I}_1} = \frac{\mu}{2}[1 - b(\bar{I}_1 - 3)]^{-2} \tag{47}$$

and

$$\frac{\partial W}{\partial J} = K\left(\frac{du}{dr} + \frac{2u}{r}\right). \tag{48}$$

By substituting the partial differentials of the energy density function (47) and (48) in the expression (46) for the stress tensor, we may write the condition for mechanical equilibrium (45) as

$$\left\{K + \frac{4\mu}{3}[1 - b(\bar{I}_1 - 3)]^{-2}\right\}\left(\frac{d^2u}{dr^2} + \frac{2}{r}\frac{du}{dr} - \frac{2u}{r^2}\right) + \frac{8\mu}{3}b[1 - b(\bar{I}_1 - 3)]^{-3}\frac{d\bar{I}_1}{dr}\left(\frac{du}{dr} - \frac{u}{r}\right) = 0. \tag{49}$$

After multiplying by $[1 - b(\bar{I}_1 - 3)]^3$ we write

$$[1 - b(\bar{I}_1 - 3)]\left\{K[1 - b(\bar{I}_1 - 3)]^2 + \frac{4\mu}{3}\right\} \times \left(\frac{d^2u}{dr^2} + \frac{2}{r}\frac{du}{dr} - \frac{2u}{r^2}\right) + \frac{8\mu}{3}b\frac{d\bar{I}_1}{dr}\left(\frac{du}{dr} - \frac{u}{r}\right) = 0. \tag{50}$$

To bring (50) to dimensionless form, we normalize the radial coordinate by the cell radius $\tilde{r} = r/R_0$ and the displacement by the displacement on the cell boundary $\tilde{u} = u/u_0$. We quantify the nonlinearity by $A = b(u_0/R_0)^2 = [(u_0/R_0)/\gamma_a]^2$, which is a measure of the ratio between the typical scale u_0/R_0 of the strain on the cell surface and the maximal shear strain $\gamma_a = 1/\sqrt{b}$ that the material can sustain. Finally, we express the ratio of bulk modulus to linear shear modulus in terms of the Poisson ratio (23), and eventually write the equilibrium condition as

$$(1 - A\tilde{I}_3)\left[\frac{1+\nu}{2(1-2\nu)}(1 - A\tilde{I}_3)^2 + 1\right]\left(\frac{d^2\tilde{u}}{d\tilde{r}^2} + \frac{2}{\tilde{r}}\frac{d\tilde{u}}{d\tilde{r}} - 2\frac{\tilde{u}}{\tilde{r}^2}\right) + 2A\frac{d\tilde{I}_3}{d\tilde{r}}\left(\frac{d\tilde{u}}{d\tilde{r}} - \frac{\tilde{u}}{\tilde{r}}\right) = 0, \tag{51}$$

where

$$\tilde{I}_3 = \left(\frac{R_0}{u_0}\right)^2(\bar{I}_1 - 3) = \frac{4}{3}\left(\frac{d\tilde{u}}{d\tilde{r}} - \frac{\tilde{u}}{\tilde{r}}\right)^2 \tag{52}$$

is a dimensionless measure of the shear in the matrix.

Equation (51) is a nonlinear second-order ordinary differential equation for the dimensionless displacement as a function of the dimensionless radius, $\tilde{u}(\tilde{r})$. We obtain $\tilde{u}(\tilde{r})$ by numerically solving the boundary value problem using our two boundary conditions: given displacement on the cell border $\tilde{u}(1) = 1$, and zero displacement, either at infinity for the unbounded geometry $\tilde{u}(\infty) = 0$ or at $\tilde{R}_1 = R_1/R_0$ for the bounded geometry $\tilde{u}(\tilde{R}_1) = 0$.

Clearly, in the limit $A = 0$ of vanishing nonlinearity, Eq. (51) reduces to Eq. (3), which describes a linearly elastic medium. In this linear limit, there are two solutions, $\tilde{u} = \tilde{r}$ and $\tilde{u} = 1/\tilde{r}^2$, and as shown in Sec. III, a linear combination of the two can match any given set of boundary conditions. More interestingly, in this spherical geometry, the solution $\tilde{u} = \tilde{r}$ that contains only compression without shear, leads to $\tilde{I}_3 = 0$ and thus solves Eq. (51) for arbitrary strength A of the nonlinearity. This solution is consistent with the first boundary condition at the cell border $\tilde{u}(1) = 1$, but it increases in magnitude with $\tilde{r}$ and thus cannot satisfy the second, zero displacement boundary condition at $\tilde{r} = \infty$ or at $\tilde{r} = \tilde{R}_1$.

B. Unbounded cell

For an unbounded cell, the dimensionless displacement $\tilde{u}(\tilde{r})$ depends only on the dimensionless strength A of the nonlinearity and on the Poisson ratio ν. The behavior of an unbounded cell in this nonlinear material model depends very weakly on the Poisson ratio [27]; thus we will not consider this dependence here, and all the numerical results we present below are for $\nu = 0.4$. As shown in Fig. 3(a), for $A = 0$ the response is completely linear, and the displacement decays according to the prediction of linear elasticity, $\tilde{u}(\tilde{r}) = 1/\tilde{r}^2$, or $u(r) = u_0(R_0/r)^2$. As A increases, an increasingly larger region near the cell responds nonlinearly, approaching the shearless solution $\tilde{u}(\tilde{r}) = \tilde{r}$, or $u(r) = u_0 r/R_0$, while far enough from the cell $\tilde{r} \gg 1$, deformations decay and the matrix restores its linear response, leading to a $\tilde{u} \propto 1/\tilde{r}^2$ decay of displacements in the far field. The far-field behavior may be written as $u(r) = u_{\text{eff}}(R_0/r)^2$, or $\tilde{u}(\tilde{r}) = \tilde{u}_{\text{eff}}/\tilde{r}^2$, where $\tilde{u}_{\text{eff}} = u_{\text{eff}}/u_0$ describes the amplification of the effective displacement on the cell border as felt at long distances. We will denote by $\tilde{R}_* \equiv R_*/R_0$ the position of the maximum of $\tilde{u}(\tilde{r})$. This position roughly divides space into the nonlinear near-field compression-dominated regime at $\tilde{r} < \tilde{R}_*$ and the linearly elastic far-field shear-dominated regime at $\tilde{r} > \tilde{R}_*$.

C. Bounded cell

To study matrix-mediated mechanical interaction between cells in a nonlinear medium, we employ the mean-field geometrical setup presented in Sec. II, which we have studied for a linear matrix in Sec. III. We now numerically solve Eq. (51) with the boundary condition $\tilde{u}(\tilde{R}_1) = 0$. In this bounded geometry, the dimensionless displacement solution $\tilde{u}(\tilde{r})$ depends not only on the Poisson ratio ν and on the dimensionless nonlinearity A, but also on the dimensionless distance $\tilde{R}_1$ between cells. We show in Fig. 3(b) numerical results for varying A and $\tilde{R}_1$.

The first thing to note in comparison to a linear medium is the following: In the unbounded geometry, the

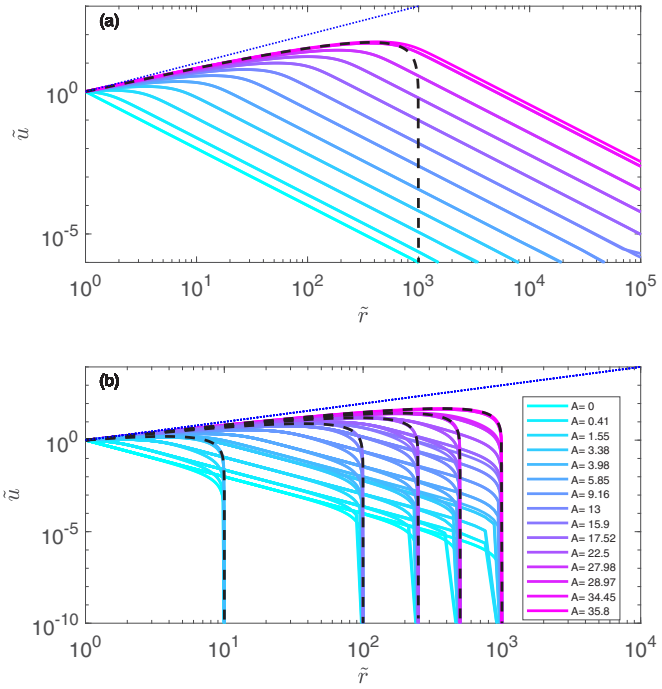

FIG. 3. Normalized displacement $\tilde{u} = u/u_0$ vs normalized radius $\tilde{r} = r/R_0$ in spherical nonlinear medium for the (a) unbounded geometry and (b) geometry bounded at $\tilde{R}_1 = R_1/R_0 = 10, 100, 250, 500, 1000$. Colors mark the dimensionless strength $A = bu_0^2/R_0^2$ of the nonlinearity, as indicated in the legend. All results are for Poisson ratio $\nu = 0.4$. In both geometries, for increasing nonlinearity, the near-field behavior tends toward the shearless solution $\tilde{u} = \tilde{r}$ represented by the blue dotted line and may be approximated by Eq. (53), which is drawn with a black dashed line only for the maximal A value for each case.

dimensionless nonlinearity A of the problem may take arbitrarily large values. This means that for a given material nonlinearity b, the displacement u_0 on the cell boundary can take any value. As seen in Fig. 3(a), increasing A causes an increase in the radius $\tilde{R}_*$ where $\tilde{u}(\tilde{r})$ crosses over from the compression-only solution $\tilde{u} = \tilde{r}$ to the shear-only solution $\tilde{u} = \tilde{u}_{\rm eff}/\tilde{r}^2$. However, for the bounded geometry, this crossover length $\tilde{R}_*$ clearly cannot be larger than $\tilde{R}_1$. This implies that for given dimensionless cell-cell distance $\tilde{R}_1$, there is a maximal value A_a that the nonlinearity can reach. Thus for given geometry specified by R_0 and R_1 and for given material nonlinearity b, the displacement u_0 on the cell boundary can increase only up to some maximal value $u_a = R_0\sqrt{A_a(\tilde{R}_1)/b}$.

In our nonlinear model (39), for large strain the resistance to shear becomes increasingly larger than the resistance to compression. Hence, in mechanical equilibrium, the shear component of the deformation tends to be minimal. For our spherical geometry, requiring $\tilde{I}_3 = 0$ leads to the solution $\tilde{u}(\tilde{r}) = \tilde{r}$, which is consistent with the boundary condition $\tilde{u}(1) = 1$, but cannot be consistent with the boundary condition $\tilde{u}(\infty) = 0$ or $\tilde{u}(\tilde{R}_1) = 0$. An approximate solution to (51) that decays in the far field is obtained by taking $\tilde{I}_3 = 1/A$ [27], which by substitution in (52) leads to

$$\tilde{u}(\tilde{r}) = \tilde{r} - \sqrt{\frac{3}{4A}}\tilde{r}\log\tilde{r}, \tag{53}$$

which in turn also causes $d\tilde{I}_3/d\tilde{r}$ to vanish. Figure 3 shows how well (53) agrees with the near-field behavior of the displacement field, both for the bounded and for the unbounded geometry.

We may approximate the maximal possible displacement u_a on the cell boundary by requiring that for A_a the approximate near-field solution (53) reaches zero at the distance $\tilde{R}_1$. The justification for this is that for $u_0 < u_a$, or correspondingly $A < A_a$, the displacement field has room to cross over at larger distances to the linear elasticity solution so that it will eventually satisfy the boundary condition $\tilde{u}(\tilde{R}_1) = 0$. For $u_0 > u_a$ on the other hand, the near-field solution (53) is still finite at $\tilde{R}_1$ and the zero-displacement boundary condition there may not be satisfied. Thus, setting $\tilde{u}(\tilde{R}_1) = 0$ in (53), we write

$$\tilde{R}_1 - \sqrt{\frac{3}{4A_a}}\tilde{R}_1\log\tilde{R}_1 = 0, \tag{54}$$

from which we obtain the maximal dimensionless nonlinearity

$$A_a = \tfrac{3}{4}\log^2\tilde{R}_1. \tag{55}$$

This lead to the maximal possible cell contraction

$$\tilde{u}_a = \frac{u_a}{R_0} = \sqrt{\frac{3}{4}}\gamma_a\log\frac{R_1}{R_0}, \tag{56}$$

which scales linearly with the maximal shear strain γ_a, and logarithmically with the dimensionless cell-cell distance. This simple theoretical prediction agrees remarkably well with our numerical results, as shown in Fig. 4(a). Note that at $A = A_a$, our approximate solution (53) becomes exact, as it satisfies the boundary conditions both at $\tilde{r} = 1$ and at $\tilde{r} = \tilde{R}_1$; see Fig. 3(b). Before moving on to discussing the interaction energy we also note that (56) may be inverted to obtain the closest distance between cells that contract by a given amount u_0,

$$\min(R_1) = R_0\exp\left(\sqrt{\frac{4}{3}}\frac{u_0/R_0}{\gamma_a}\right), \tag{57}$$

or alternatively

$$\min(\tilde{R}_1) = \exp\left(\sqrt{\frac{4A}{3}}\right). \tag{58}$$

D. Interaction energy

To calculate the interaction energy for given cell size R_0, cell-cell distance R_1, material nonlinearity b, and cell contraction u_0, we need to first numerically solve the boundary value problem to get the displacement field $u(r)$ for the bounded and for the unbounded geometries for any intermediate cell contraction $0 < w < u_0$. Then we use u and du/dr at R_0 to evaluate the radial stress (46) $\tau(w) = \sigma_{rr}(R_0)$ on the cell surface. Finally, we numerically integrate Eq. (1) to obtain the elastic energy stored in the medium for the bounded and for the unbounded cases, and subtract them to get the interaction energy.

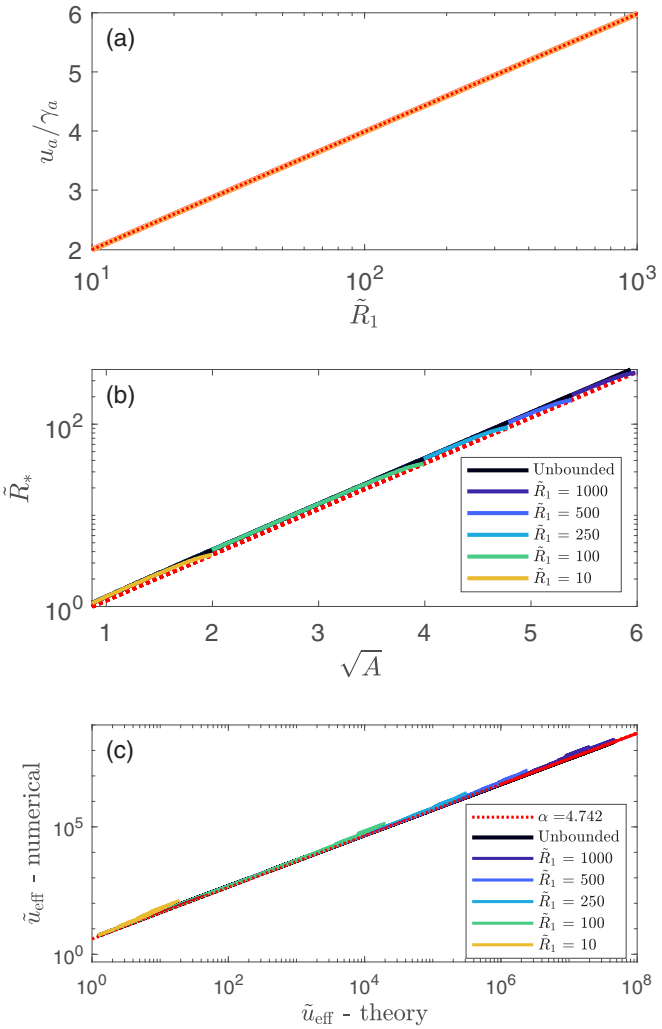

FIG. 4. (a) Maximal possible cell contraction increases with cell-cell distance according to Eq. (56). Numerical results for $b = 0.1, 0.5, 0.8, 1.1, 2, 5, 10$ all collapse to a single curve, which perfectly agrees with the theoretical prediction. (b) Position of maximal displacement increases with dimensionless nonlinearity according to Eq. (59) both for the bounded and for the unbounded geometries. (c) Effective far-field displacement increases with A and decreases with $\tilde{R}_1$ following Eq. (61). In all panels, theoretical prediction is marked with a red dotted line.

1. Displacement regulation

The numerical results of ΔE vs u_0 for various values of b and R_1 are given in Fig. 5. For small u_0, the material responds linearly; thus the interaction energy grows quadratically with u_0, as predicted in a linear medium. For increasing u_0, the interaction energy grows more rapidly and diverges at a finite contraction u_a, which depends on R_1 and on b according to (56). We first note that the dependence of ΔE on the material nonlinearity b may be scaled out if we normalize ΔE by the interaction energy (15) that we would get for these values of u_0, R_0 and R_1 in a linear medium. Figure 6 shows that after this normalization, and by also scaling u_0 by its maximal possible value u_a in the nonlinear case, we obtain collapse of the results for different b values to master curves that depend only on $\tilde{R}_1 = R_1/R_0$.

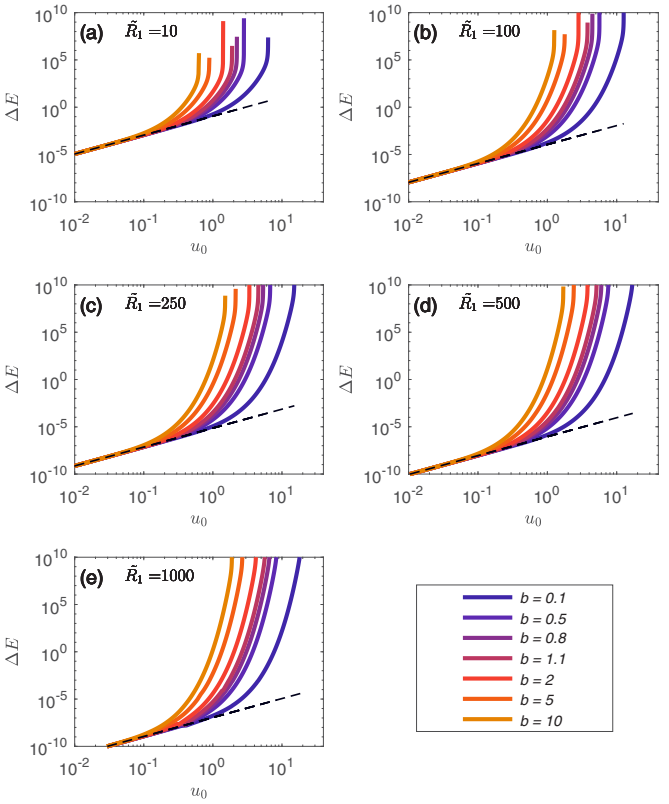

FIG. 5. Interaction energy vs cell contraction for different values of R_1 and b. Interaction energy is scaled by μR_0, and cell displacement is scaled by R_0. Black dashed lines are linear elasticity behavior for $b = 0$.

To approximate the entire dependence on u_0 as well as the dependence on $\tilde{R}_1$, we first note that the near-field

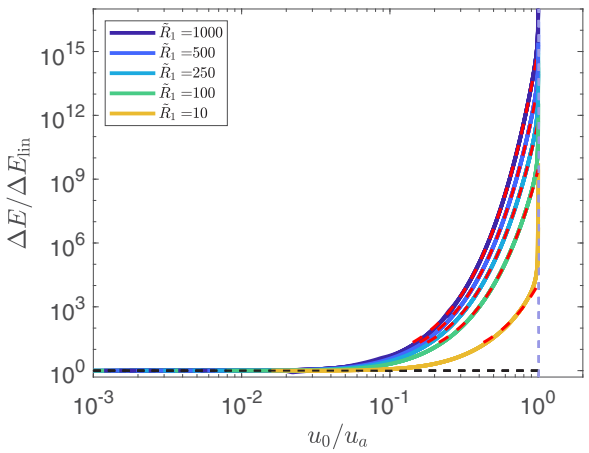

FIG. 6. Scaled interaction energy behaves according to linear elasticity (15) for small cell contraction (black dashed line). As u_0 approaches u_a, the interaction energy grows according to Eq. (63) (red dashed lines), until it diverges at $u_0 = u_a$ (blue dashed line). Results for different values of the material nonlinearity b collapse to curves that depend only on $\tilde{R}_1$.

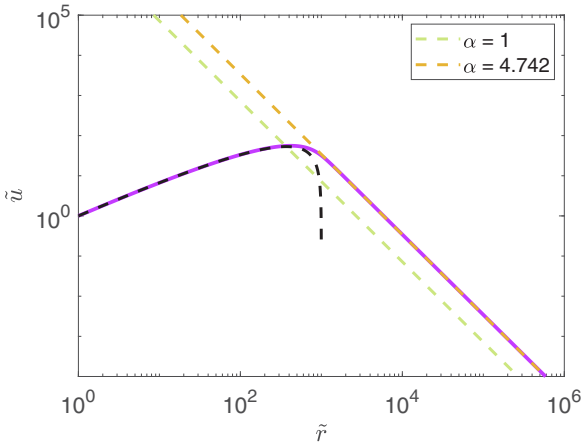

FIG. 7. Crossover of $\tilde{u}(\tilde{r})$ from near-field behavior of Eq. (53) (dashed black line) to far-field $\tilde{u} = \tilde{u}_{\rm eff}/\tilde{r}^2$ behavior. Matching the two solutions at $\tilde{R}_*$ (green dashed line) underestimates $\tilde{u}_{\rm eff}$. Matching at a slightly larger distance (orange dashed line) is obtained by taking $\alpha > 1$ in Eq. (61). Results are shown for $A = 35.7858$.

approximate solution (53) is maximal at

$$\tilde{R}_* = \exp\left(\sqrt{\frac{4A}{3}} - 1\right). \tag{59}$$

This agrees very well with the position of the maximum of $\tilde{u}(\tilde{r})$ as obtained from our numerical solution, both for bounded and for unbounded geometries; see Fig. 4(b). Note that (53) has a local maximum at $\tilde{r} > 1$ only for $A > 3/4$; thus all the analysis that follows is relevant only for dimensionless nonlinearity that is larger than this level. Now, in the far field, we expect the solution (12) in a linear medium to hold, but with the displacement u_0 on the surface of the cell replaced by some larger, effective displacement $u_{\rm eff}$. In dimensionless form this reads

$$\tilde{u}(\tilde{r}) = \frac{\tilde{u}_{\rm eff}}{\tilde{R}_1^3 - 1}\left(\frac{\tilde{R}_1^3}{\tilde{r}^2} - \tilde{r}\right). \tag{60}$$

As has successfully been done for the unbounded geometry [27], also for our bounded geometry, the dimensionless effective displacement may be obtained by matching the near-field solution (53) and the far-field solution (60) at $\tilde{R}_*$ (59). The crossover between these two solutions is not sharp but exists over a certain crossover region; see Fig. 7. Thus we allow for a dimensionless multiplicative factor α between the two solutions at $\tilde{R}_*$. This leads to

$$\tilde{u}_{\rm eff} = \frac{u_{\rm eff}}{u_0} = \alpha\sqrt{\frac{3}{4A}}\frac{\tilde{R}_1^3 - 1}{\frac{\tilde{R}_1^3}{\tilde{R}_*^3} - 1}. \tag{61}$$

For $\tilde{R}_1 \gg \tilde{R}_*$ this reduces to $\tilde{u}_{\rm eff} = \alpha\sqrt{3/(4A)}\tilde{R}_*^3$. Note that (61) cannot explain the divergence of ΔE as u_0 approaches u_a since it is not singular at the maximal cell contraction A_a; it is just equal to

$$\tilde{u}_{\rm eff} = \alpha\frac{\tilde{R}_1^3 - 1}{\log\tilde{R}_1(e^3 - 1)}. \tag{62}$$

Figure 4(c) shows the remarkable agreement of (61) with the numerical results and identifies the value $\alpha \approx 4.7$ for all the values of b and $\tilde{R}_1$ considered.

The near-field behavior of the displacement field is very similar in the bounded and in the unbounded geometries, and most of the differences between the two cases are in the far field (see Fig. 3). Thus we assume that most of the contribution to the difference in the elastic energy stored in the medium between the two geometries comes from the far-field region. This enables us to approximate the interaction energy as the difference in energies stored in a linearly elastic medium displaced by $u_{\rm eff}$ rather than by u_0 at the cell boundary. Thus we substitute $u_{\rm eff}$ of the bounded geometry instead of u_0 in Eq. (15) for ΔE, and get

$$\Delta E = \Delta E_{\rm lin}\tilde{u}_{\rm eff}^2 \tag{63}$$

where $\Delta E_{\rm lin}$ is the interaction energy in a linear medium (15). Figure 6 shows the impressive agreement of this theoretical expression with the numerical results up until very close to the divergence of ΔE at u_a.

2. *Stress regulation*

We now numerically evaluate the radial stress (46) on the surface of the cell for the unbounded and for the bounded geometries, and subtract the corresponding energies at given stress to obtain the interaction energy for the situation in which the cell regulates the stress on its surface regardless of its mechanical environment. For simplicity, for cells in a nonlinear matrix we will assume that the cell does not resist the deformation and that all the active force applied by the cell is directed toward generating stress in the matrix. Namely $\sigma_c = 0$ and $\sigma_0 = -\sigma_m$. When relating this to the linear elasticity solution (20), this is obtained by setting $K_c = 0$.

The reasoning explaining why for displacement regulation the interaction energy is positive (repulsion) and for stress regulation it is negative (attraction) is valid also for cells in a strain-stiffening matrix. Our numerical calculations indeed result in positive interaction energy for displacement regulation and negative interaction energy for stress regulation. For displacement regulation we saw that the divergence of the shear stress at a finite strain γ_a [see Fig. 2(a)] causes the interaction energy to diverge at a finite displacement u_a. For stress regulation on the other hand, at least from the point of view of the matrix resistance, the active stress that the cell generates can be arbitrarily large [see Fig. 2(b)].

When plotting in Fig. 8 the numerically obtained interaction energy versus the regulated stress we see the linear-elasticity $\Delta E \propto -\sigma_0^2$ behavior (20) at low stress. This is followed by a more complex crossover at intermediate nonlinearity, and eventually at extremely large stress the interaction energy again scales as σ_0^2, enabling arbitrarily large values of the stress, as expected. Interestingly, we obtain the quadratic scaling $\Delta E \propto \sigma_0^2$ not only in the linear regime but also in the strongly nonlinear regime. This may be explained from the fact that the nonlinear dependence of $u_{\rm eff}$ on u_0 and of σ_0 on $u_{\rm eff}$ are reciprocal such that $\sigma_0 \propto u_{\rm eff}$ [27]. Combining this with the result presented above that $\Delta E \propto u_{\rm eff}^2$ leads to $\Delta E \propto \sigma_0^2$. Impressively, when we scale the nonlinear interaction energy by the linear result, and scale the stress

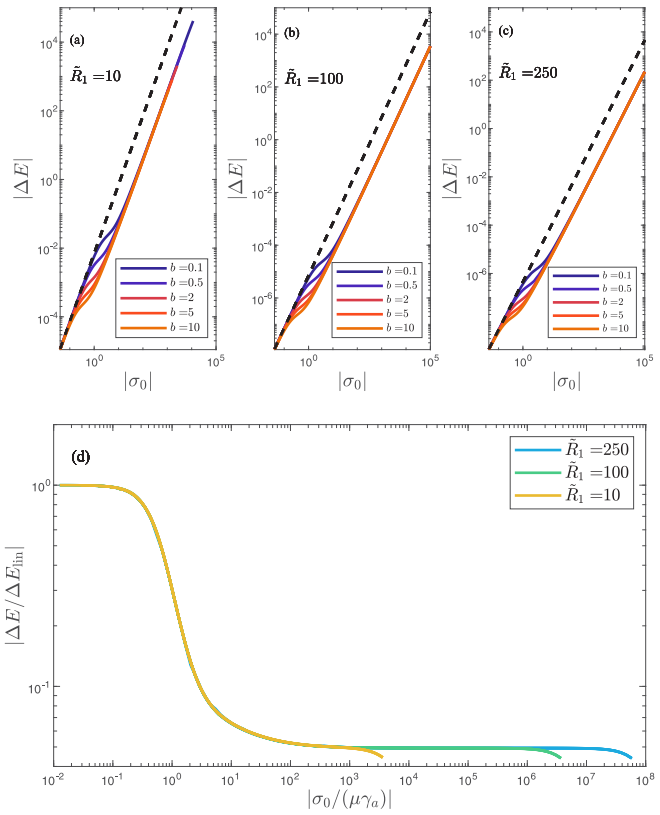

FIG. 8. Interaction energy with stress regulation in a nonlinear medium. (a–c) Results for different values of $\tilde{R}_1$ and b. Dashed black lines are linear elasticity behavior (20). Interaction energy is scaled by μ/R_0^3 and stress is scaled by μ. (d) When normalizing the interaction energy by the linear prediction and normalizing the stress by the typical stress $\mu\gamma_a$ where strain stiffening becomes dominant, results for all b and $\tilde{R}_1$ collapse to a single curve.

by the typical stress $\mu\gamma_a$ where the strain stiffening becomes significant, all the numerical results collapse to a single curve, as shown in Fig. 8(d) for multiple values of $\tilde{R}_1$ and b.

V. DISCUSSION

In this paper, we used a mean-field approach to study matrix mediated interactions between contracting biological cells in linear and in nonlinear elastic surroundings. We showed how the regulatory behavior of the cell's mechanical activity always gives rise to repulsion when displacement is regulated and to attraction when stress is regulated. For displacement regulation, the interaction does not depend on the rigidity of the cell. For stress regulation, it depends only on the bulk modulus of the cell in spherically symmetric situations, while in cylindrical setups it depends also on its shear modulus. For a nonlinear, shear-stiffening matrix, the interaction energy diverges at a finite displacement, while for stress regulation the stress may be arbitrarily large. It is still not entirely clear what is the regulatory mechanical activity of live cells and what biological mechanism determines it. There is much evidence for stress regulation, however, as well as some indications of situations in which displacement is regulated [36–40,47,48].

For simplicity, we treated the cell as a passive, linearly elastic solid. This is clearly a very crude description, and the way that cells set their size, displacement, and forces includes many further processes; see, e.g., [49,50]. However, we emphasize that for displacement regulation the mechanical response of the cell is irrelevant for the interaction energy. Namely, no matter how complicated is the response of the cell, if we consider the situation in which cells regulate the displacement they generate, then the inside of the cell behaves exactly the same regardless of the distance to neighboring cells, and our results both for a linearly elastic matrix and for a nonlinear matrix are valid also beyond the simplified assumption that the cell is a passive, linearly elastic solid. In the case of stress regulation, our analytical results for a linearly elastic matrix rely on the linearity assumption for the cell, whereas for a nonlinear matrix we assumed that the cell is much softer than the matrix, and therefore its mechanical response does not affect the interaction with other cells.

We focused our nonlinear material model for the extracellular matrix on shear stiffening and included nonlinearity only in the resistance to shear. It would be interesting to study the interactions and different regulatory behaviors that we consider also in models that take into account the anisotropy of the matrix [28,30,51], that include also nonlinearity in the compressive response, and in models that take into account the discrete fibrous nature of the biopolymer gel comprising the extracellular environment [31,32,35,51–53]. We note that our mean-field description of cell-cell interactions may also be employed in order to study the response to spatial variations in matrix rigidity. Specifically, it would be interesting to extend the analysis regarding durotaxis performed in Ref. [29] also to cylindrical geometry and to nonlinear media. Finally, our theoretical work could motivate experimental studies to investigate matrix-mediated interactions between contractile force dipoles and to decipher the regulatory behavior of live cells.

ACKNOWLEDGMENTS

We thank D. Ben-Yaakov, R. Golkov, S. Goren, Y. Koren, A. Lesman, S. Safran, O. Tchaicheeyan, and X. Xu for fruitful discussions. This research was supported in part by a grant from the United States–Israel Binational Science Foundation, by the Israel Science Foundation Grant No. 968/16 and by the National Science Foundation Grant No. NSF PHY-1748958.

[1] U. S. Schwarz and S. A. Safran, Rev. Mod. Phys. **85**, 1327 (2013).
[2] A. Engler, S. Sen, H. Sweeney, and D. Discher, Cell **126**, 677 (2006).
[3] M. Poujade, E. Grasland-Mongrain, A. Hertzog, J. Jouanneau, P. Chavrier, B. Ladoux, A. Buguin, and P. Silberzan, Proc. Natl. Acad. Sci. USA **104**, 15988 (2007).
[4] D. Montell, Nat. Rev. Mol. Cell Biol. **4**, 13 (2003).

[5] A. Lesman, J. Notbohm, D. A. Tirrell, and G. Ravichandran, J. Cell Biol. **205**, 155 (2014).

[6] A. Abuhattum, A. Gefen, and D. Weihs, Integr. Biol. **7**, 1212 (2015).

[7] P. Friedl and D. Gilmour, Nat. Rev. Mol. Cell Biol. **10**, 445 (2009).

[8] N. Gal and D. Weihs, Cell Biochem. Biophys. **63**, 199 (2012).

[9] D. Gomez, S. Natan, Y. Shokef, and A. Lesman, Adv. Biosys. **3**, 1900192 (2019).

[10] D. Gomez, E. Teomy, A. Lesman, and Y. Shokef, New J. Phys. **22**, 103008 (2020).

[11] W.-H. Jung, N. Yam, C.-C. Chen, K. Elawad, B. Hu, and Y. Chen, Biomaterials **234**, 119756 (2020).

[12] C. A. Reinhart-King, M. Dembo, and D. A. Hammer, Biophys. J. **95**, 6044 (2008).

[13] J. P. Winer, S. Oake, and P. A. Janmey, PLoS ONE **4**, e6382 (2009).

[14] A. Buxboim, K. Rajagopal, A. E. X. Brown, and D. E. Discher, J. Phys.: Condens. Matter **22**, 194116 (2010).

[15] H. Mohammadi, P. A. Janmey, and C. A. McCulloch, Biomaterials **35**, 1138 (2014).

[16] J. Notbohm, A. Lesman, P. Rosakis, D. A. Tirrell, and G. Ravichandran, J. R. Soc. Interface **12**, 20150320 (2015).

[17] J. Notbohm, A. Lesman, D. A. Tirrell, and G. Ravichandran, Integr. Biol. **7**, 1186 (2015).

[18] U. S. Schwarz and S. A. Safran, Phys. Rev. Lett. **88**, 048102 (2002).

[19] K. Lau and W. Kohn, Surf. Sci. **65**, 607 (1977).

[20] N. Q. Balaban, U. S. Schwarz, D. Riveline, P. Goichberg, G. Tzur, I. Sabanay, D. Mahalu, S. Safran, A. Bershadsky, L. Addadi, and B. Geiger, Nature Cell Biol. **3**, 466 (2001).

[21] J. P. Butler, I. M. Tolić-Nørrelykke, B. Fabry, and J. J. Fredberg, Am. J. Physiol. Cell Physiol. **282**, C595 (2002).

[22] I. B. Bischofs and U. S. Schwarz, Proc. Natl. Acad. Sci. USA **100**, 9274 (2003).

[23] I. B. Bischofs, S. A. Safran, and U. S. Schwarz, Phys. Rev. E **69**, 021911 (2004).

[24] I. B. Bischofs and U. S. Schwarz, Phys. Rev. Lett. **95**, 068102 (2005).

[25] I. B. Bischofs and U. S. Schwarz, Acta Biomater. **2**, 0510391 (2006).

[26] R. Golkov and Y. Shokef, Phys. Rev. E **99**, 032418 (2019).

[27] Y. Shokef and S. A. Safran, Phys. Rev. Lett. **108**, 178103 (2012); **109**, 169901(E) (2012).

[28] X. Xu and S. A. Safran, Phys. Rev. E **92**, 032728 (2015).

[29] D. Ben-Yaakov, R. Golkov, Y. Shokef, and S. A. Safran, Soft Matter **11**, 1412 (2015).

[30] H. Wang and X. Xu, Soft Matter **16**, 10781 (2020).

[31] S. Natan, Y. Koren, O. Shelah, S. Goren, and A. Lesman, Mol. Biol. Cell **31**, 1474 (2020).

[32] J. Kim, J. Feng, C. A. R. Jones, X. Mao, L. M. Sander, H. Levine, and B. Sun, Nat. Commun. **8**, 842 (2017).

[33] J. N. Israelachvili, *Intermolecular and Surface Forces* (Academic Press, London, 1992).

[34] R. Golkov and Y. Shokef, New J. Phys. **19**, 063011 (2017).

[35] R. S. Sopher, H. Tokash, S. Natan, M. Sharabi, O. Shelah, O. Tchaicheeyan, and A. Lesman, Biophys. J. **115**, 1357 (2018).

[36] R. Brown, R. Prajapati, D. McGrouther, I. Yannas, and M. Eastwood, J. Cell. Physiol. **175**, 323 (1998).

[37] T. M. Freyman, I. V. Yannas, R. Yokoo, and L. J. Gibson, Exp. Cell. Res. **272**, 153 (2002).

[38] A. Saez, A. Buguin, P. Silberzan, and B. Ladoux, Biophys. J. **89**, L52 (2005).

[39] M. Ghibaudo, A. Saez, L. Trichet, A. Xayaphoummine, J. Browaeys, P. Silberzan, A. Buguin, and B. Ladoux, Soft Matter **4**, 1836 (2008).

[40] R. De, A. Zemel, and S. A. Safran, Biophys. J. **94**, L29 (2008).

[41] S. He, Y. Su, B. Ji, and H. Gao, J. Mech. Phys. Solids **70**, 116 (2014).

[42] A. Bower, *Applied Mechanics of Solids* (CRC Press, Boca Raton, FL, 2009).

[43] M. L. Gardel, J. H. Shin, F. C. MacKintosh, L. Mahadevan, P. Matsudaira, and D. A. Weitz, Science **304**, 1301 (2004).

[44] C. Storm, J. J. Pastore, F. C. MacKintosh, T. C. Lubensky, and P. A. Janmey, Nature (London) **435**, 191 (2005).

[45] D. Vader, A. Kabla, D. Weitz, and L. Mahadevan, PLoS ONE **4**, e5902 (2009).

[46] C. P. Broedersz and F. C. MacKintosh, Rev. Mod. Phys. **86**, 995 (2014).

[47] A. K. Yip, K. Iwasaki, C. Ursekar, H. Machiyama, M. Saxena, H. Chen, I. Harada, K. H. Chiam, and Y. Sawada, Biophys. J. **104**, 19 (2013).

[48] D. Stamenović and M. L. Smith, Soft Matter **16**, 6946 (2020).

[49] R. M. Adar and S. A. Safran, Proc. Natl. Acad. Sci. USA **117**, 5604 (2020).

[50] B. L. Doss, M. Pan, M. Gupta, G. Grenci, R.-M. Mège, C. T. Lim, M. P. Sheetz, R. Voituriez, and B. Ladoux, Proc. Natl. Acad. Sci. USA **117**, 12817 (2020).

[51] S. Goren, Y. Koren, X. Xu, and A. Lesman, Biophys. J. **118**, 1152 (2020).

[52] H. Wang, A. S. Abhilash, C. S. Chen, R. G. Wells, and V. B. Shenoy, Biophys. J **107**, 2592 (2014).

[53] F. Alisafaei, X. Chen, T. Leahy, P. A. Janmey, and V. B. Shenoy, Soft Matter **17**, 241 (2021).